Measurement 135 (2019) 406–412

Contents lists available at ScienceDirect

Measurement

journal homepage: www.elsevier.com/locate/measurement

Small-sized visual angular displacement measurement technology

Xingdan Jia [a,b], Qiuhua Wan [a,*], Hai Yu [a,*], Xinran Lu [a], Changhai Zhao [a]

[a] Changchun Institute of Optics, Fine Mechanics and Physics, Chinese Academy of Sciences, Changchun 130033, China
[b] University of Chinese Academy of Sciences, Beijing 100049, China

ARTICLE INFO

Article history:
Received 18 April 2018
Received in revised form 4 October 2018
Accepted 18 November 2018
Available online 19 November 2018

Keywords:
Image detector
Varying principle
High-precision
High-resolution

ABSTRACT

Visual angular displacement measurement methods are a popular approach to photoelectric displacement measurement technology, as they provide significantly higher precision than traditional angular displacement measurement methods. This paper proposes a small-sized high-precision angular displacement measurement technology based on the sub-pixel level varying principle. The small-sized visual angular displacement measurement mechanism is first established without lens near-field imaging. A coding method based on the varying principle is then developed in order to decrease the ruled grating density. A sub-pixel angular displacement calculating model based on uniline pix is built to decrease the pixel data and enhance the frequency response of the measurement system; the corresponding data combination and correction algorithms are proposed. The error analysis is proposed. Tests on an angular displacement measurement device prototype showed a resolution of 20-bit and precision of 20.4″. The device also outperformed traditional angular displacement measuring devices of similar size, but features low ruled grating density and miniaturization. The results presented here may thus provide a workable foundation for further research on small-size visual angular displacement measurement devices.

1. Introduction

Photoelectrical angular displacement measurement devices represent an innovative combination of optical, mechanical, and electronic functions [1,2]. They are often used in fine photoelectric displacement measurement applications; they feature high precision, high resolution, and excellent stability.

In traditional angular displacement measurement techniques, relative displacement of the calibration grating and the indication grating is typically utilized to generate a moiré signal as shown in Fig. 1. The moiré fringe signal is collected by photosensitive elements, and amplified and shaped into the processor to realize angular displacement calculation.

Under traditional angular displacement measurement methodology, high-precision, high-resolution angular displacement measurement is achieved by increasing the grating scribe density. An overly dense grating reticle will result in insufficient throughput, however, or interference among adjacent code channels resulting in decoder failure. The traditional measurement device also requires a large disk to function properly, thus, the size of the whole device is generally large. General advancements in technology have brought about increasingly stringent requirements for photoelectrical angular displacement measurement devices. They must be highly precise and with high resolution, but also must be suitable for miniaturization [3,4]. Advancements in digital image processing technology have allowed for new image detectors which measure angular displacement with smaller disks at similar precision and resolution [5–7,20–22].

Visual angular displacement measurement has become a popular topic among fine photoelectric displacement measurement technology researchers. The NASA Space Agency (USA) took the lead in researching high-precision image angular displacement devices at resolution up to 0.01″ [8]. The Changchun Institute of Optics, Fine Mechanics and Physics built a 21-bit measuring device with a lens recently; its precision is 6.33″ [18]. Scholars in the U.S. [8–10], Japan [11,12], Spain [13,14], Korea [15], and China [16–18] have also made remarkable achievements in this regard. Some have achieved high-resolution angular displacement measurement via different code encoding method [10,11,15,16]; Some researchers have explored the optical systems of these devices in effort to improve performance of measurement device [19]; others have attempted to enhance device reliability via different error compensation algorithms [12,18]. However, most of the extant research is based on lens magnification and applies multiple circles to the disks, resulting in an oversize device.

This paper proposes novel a small-size high-resolution absolute angular displacement measurement technology based on the sub-

* Corresponding authors.
E-mail addresses: wanqh@ciomp.ac.cn (Q. Wan), yuhai@ciomp.ac.cn (H. Yu).

https://doi.org/10.1016/j.measurement.2018.11.055
0263-2241/

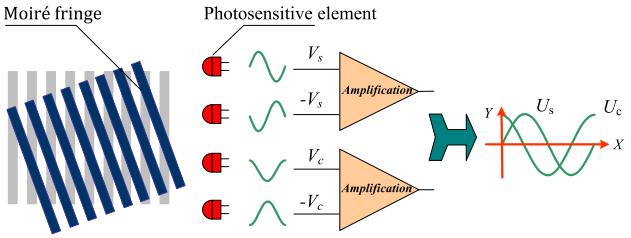

Fig. 1. Schematic diagram: Signal acquisition in traditional angular displacement measuring device.

pixel varying principle. We determined the small-image angular displacement measurement principle, then built a sub-pixel angular displacement calculating model, data combination algorithm, and code correction method. We also conducted an error analysis. We designed an angular displacement measurement device prototype and subjected it to contrast tests. The resolution of the device reached 20-bit and its accuracy reached 20.40″. In other words, the prototype outperformed traditional angular displacement measurement devices of similar size.

The remainder of this paper is organized as follows: In Section 2, the small-image-type angular displacement measurement principle is described and our disk coding schemes are explained. Section 3 presents our sub-pixel angular displacement measurement model, angular information combined algorithm, and code correction method. Section 4 presents our error analysis. In Section 5, the measurement device prototype is discussed and our test results are reported. Section 6 provides a brief summary and conclusion.

2. Small-image-type angular displacement measurement principle

2.1. Small-image angular displacement measurement device structure

Small-image angular displacement measurement is a relatively new method which uses an image detector instead of the traditional photoelectric transducer element to identify the disk and measure the angular displacement. Using a lens for amplification disk imaging necessitates a large-size device, comes with inferior vibration resistibility, and readily offsets the feed at high or low temperature. Here, we use a non-lens near-field imaging process for angular displacement measurement.

The lens-free photographic angular displacement measurement system is shown in Fig. 2.

Fig. 2 shows the axis, light, disk, image detector, and image processing circuit of the measurement system. To achieve lens-free near-field imaging, there is a minimal gap between the disk and image detector so that the image detector clings to disk. Parallel light is applied as a light source to prevent fuzzy edges otherwise caused by light diffraction. The detector can detect sharp-edged and gray uniform images of the disk.

The disk is coded by a varying principle. Parallel light pours in through the disk, then the detector obtains a disk image. The light transmission region and "marking lines" on the disk are determined according to the pixel values, then the sub-pixel angular displacement and decoding characteristics are calculated by the varying principle to determine the current angular position.

2.2. Disk coding schemes

In most previous studies on this subject, the disk is coded by multiple code-track technology. If the measurement reaches 20-bit resolution, the disk is ruled with at least eight circles as-influenced by the ruling process and diffraction of light. To ensure sufficient resolution, the disk and size of the angular displacement measurement device must be enlarged. Here, we propose a varying coding method to reduce the size of the angular displacement measurement device. Fig. 3 shows a diagram of the disk coding method and image detector collecting window.

In Fig. 3, L is the reference line of the image detector. The datum track (D), auxiliary track (A), and correcting track (C) are led in to achieve absolute angular position measurement. To properly apply the image detector, every circle track is ruled by "marking lines" which are equally wide and equally spaced within the same circle track. Every track consists of equidistant marking lines distributed radially around the circumference of the disk. The datum track (D) is engraved with2^N marking lines in the circumference; the auxiliary track (A) is engraved with 2^N-1 marking lines in the circumference.

When the disk rotates with the axis, absolute angular displacement measurement is realized by identifying variations in the angular position of the reference line L. In the circumference of disk, the absolute angular position of the image detector reference line L on the datum track (D) is as follows:

$$\theta = \frac{360^\circ}{2^N} \times p + \omega_D. \tag{1}$$

In Eq. (1), p is the number of the complete grating cycles on the datum track (D) between the absolute angular position of reference line L and the absolute zero position. ω_D is the angular displacement corresponding to the incomplete grating circumference at the datum track (D). Similarly, the absolute angular position of the image detector reference line L on the auxiliary track (A) can be expressed as follows:

$$\theta = \frac{360^\circ}{2^N - 1} \times q + \omega_A. \tag{2}$$

where q is the number of complete grating cycles on the auxiliary track (A) between the absolute angular position of reference line L and the absolute zero position; ω_A is the angular displacement corresponding to the incomplete grating circumference at the auxiliary track (A).

The difference of ω_D and ω_A is:

$$\Delta\omega_1 = \omega_D - \omega_A = \frac{360^\circ}{2^N - 1} \times q - \frac{360^\circ}{2^N} \times p. \tag{3}$$

After simplification, Eq. (3) can be expressed as follows:

$$\Delta\omega_1 = \frac{360^\circ}{\left(2^N - 1\right) \times 2^N} \left[p - (p - q) \times 2^N\right]. \tag{4}$$

The grating cycle of the datum track (D) differs by one from the grating period of the auxiliary track (A), so the number of complete grating cycles p is equal to q. After simplification, Eq. (4) can be expressed as follows:

$$\Delta\omega_1 = \frac{360^\circ}{\left(2^N - 1\right) \cdot 2^N} \times p. \tag{5}$$

Eq. (5) indicates that $\triangle\omega_1$ and p are proportional in the rotation cycle, $p = \{0,1 \ldots 2^N - 1\}$. N-bit absolute angular displacement can be achieved based on $\triangle\omega_1$.

In practice, there is a certain amount of error jitter in the low-bit of $\triangle\omega_1$. Therefore, the angular position cannot be measured independently according to the datum track (D) and the auxiliary track (A). The correcting track (C) is introduced to resolve this problem in which 2^N–2^M marking lines are engraved in the circumference of the track. The absolute angular position of the image detector reference line L on the correcting track (C) can be represented as follows:

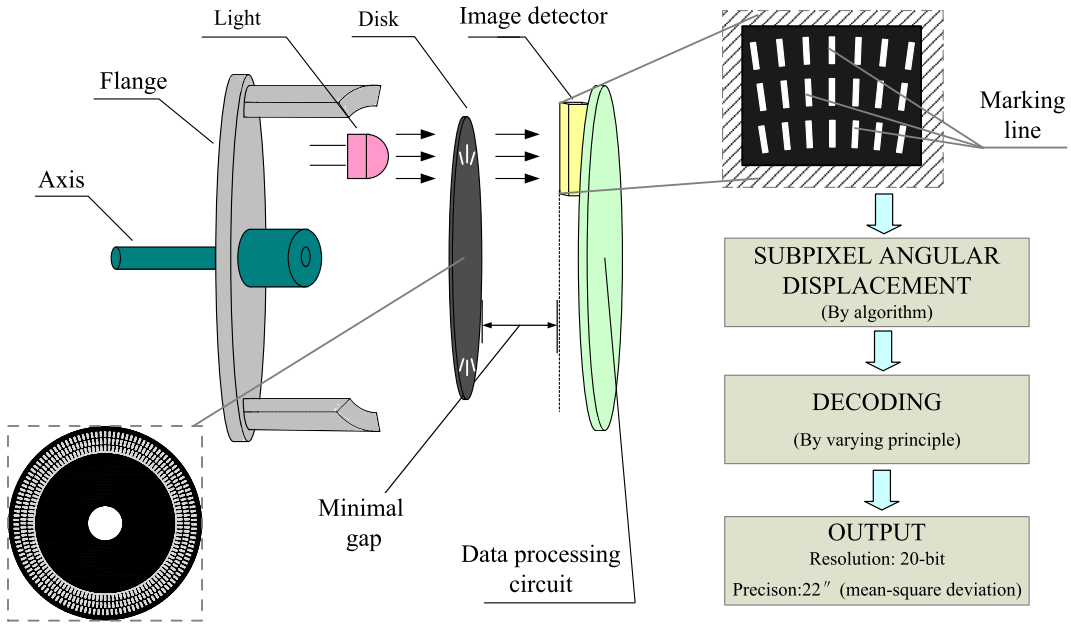

Fig. 2. Visual angular displacement measurement device principle.

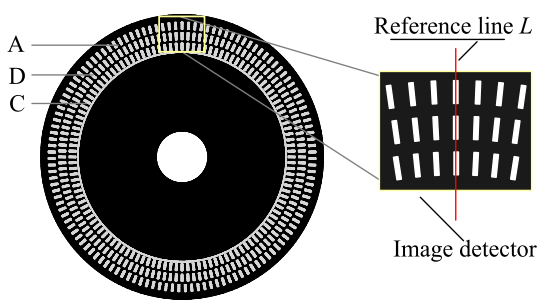

Fig. 3. Disk diagram.

$$\theta = \frac{360^\circ}{2^N - 2^M} \times r + \omega_C. \tag{6}$$

where r is the number of complete grating cycles on the correcting track (C) between the absolute angular position of reference line L and the absolute zero position; ω_C is the angular displacement corresponding to the incomplete grating circumference at the correcting track (C). The difference of ω_D and ω_C is:

$$\Delta\omega_2 = \omega_D - \omega_C = \frac{360^\circ}{2^N - 2^M} \times r - \frac{360^\circ}{2^N} \times p. \tag{7}$$

After simplification, Eq. (7) can be rewritten as follows:

$$\Delta\omega_2 = \frac{360^\circ}{\left(2^N - 2^M\right) \cdot 2^N}\left[p \times 2^M - (p - r) \times 2^N\right]. \tag{8}$$

In the rotation cycle of the grating disk, the grating cycle of the datum track (D) differs by 2^M from the grating cycle of the correcting track (C). Therefore, p and r have the following relationship:

When $p \in \left\{0, \cdots, \left(1 \times \frac{2^N}{2^M} - 1\right)\right\} p - r = 0$

When $p \in \left\{1 \times \frac{2^N}{2^M}, \cdots, \left(2 \times \frac{2^N}{2^M} - 1\right)\right\} p - r = 1$

When $p \in \left\{2 \times \frac{2^N}{2^M}, \cdots, \left(3 \times \frac{2^N}{2^M} - 1\right)\right\} p - r = 2$

When $p \in \left\{\left(2^M - 1\right) \times \frac{2}{2^M}, \left(2^M \times \frac{2^N}{2^M} - 1\right)\right\}, p - r = 2^M - 1$.

In the circumference, $p-r = \{0,1\ldots 2^{M-1}\}$. There are 2^M corresponding absolute angular positions for any $\triangle\omega_2$. Per$\triangle\omega_2$, the circumference can be divided into 2^M areas; therefore, the circumference can be divided into 2^M zones by $\triangle\omega_2$ and (N-M)-bit absolute angular displacement measurement can be realized in each zone.

Combining $\triangle\omega_1$ and $\triangle\omega_2$ can yield precise N-bit angular position information. Higher M-bit angular position information may be confirmed based on $\triangle\omega_1$; lower (N-M)-bit angular position information is confirmed based on $\triangle\omega_2$. To this effect, introducing the correcting track (C) resolves the problem of low resolution caused by the numerical jitter of $\triangle\omega_1$.

3. Angular displacement measurement algorithm

3.1. Sub-pixel angular displacement measurement model

Previous studies on small-sized angular displacement measurement are generally based on the pixel level, which strictly limits the accuracy of the measurement device due to the resolution of the image detector. In this study, we established a sub-pixel angular displacement measurement model to achieve sub-pixel angular displacement measurement and improve the measurement accuracy of the traditional detector.

On the datum track (D), 2^N marking lines are uniformly engraved in the radial direction along the circumference. The angular displacement model corresponds to the incomplete grating circumference on the datum track (D) as the disk rotates, as shown in Fig. 4.

In Fig. 4, L is the reference line of image detector, A and B are centroid of the two marking lines at the sides of the reference line L, ω_D is the angular displacement corresponding to the incomplete grating circumference, and α is the grating spacing, $\alpha = \frac{360^\circ}{2^N}$. A row

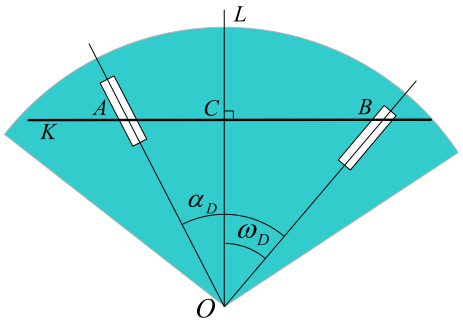

Fig. 4. Angular displacement calculation model.

of pixels can be applied to calculate the detecting line K to reduce the calculation work and improve the frequency. We first identify the area of the marking lines, apply the centroid-algorithm to calculate the centroid and achieve sub-pixel locations, and then determine the location of the centroid A、B as follows:

$$U = \frac{\sum_{i\in Z} p(x_i) \times x_i}{\sum_{i\in Z} p(x_i)}. \tag{9}$$

where $\{Z\}$ is the range of the area where the marking lines are located, i is the i-th pixel within the area $\{Z\}$, and $i\in\{Z\}$, x_i is the position of pixels within the marking line area $\{Z\}$; $p(x_i)$ represents the pixel value at position x_i. The positions of centroid A and B are calculated via Eq. (9) as U_A and U_B, respectively. The reference L is located at U_C (which is known).

Therefore, in $\triangle BOC$:

$$BC = U_B - U_C. \tag{10}$$

and ω_D is calculated as follows:

$$\omega_D = \frac{180^\circ}{\pi}\arctan\frac{BC}{OC} = \frac{180^\circ}{\pi}\arctan\frac{U_B - U_C}{OC}. \tag{11}$$

Map the angular displacement to the interval [0,1], then:

$$\eta_D = \frac{\omega_D}{\alpha} = \frac{2^N \times \omega_D}{360^\circ}. \tag{12}$$

Plug Eq. (11) into Eq. (12) and derive:

$$\eta_D = \frac{2^N}{2\pi}\arctan\frac{U_B - U_C}{OC}. \tag{13}$$

where OC is the distance of the detection line from the axial center, which is known; the angular displacement η_D can be obtained according to BC to complete the sub-pixel level angular displacement measurement.

Similarly, η_A and η_C corresponding to ω_A and ω_C can be calculated as follows:

$$\eta_A = \frac{\omega_A}{\alpha_A} = \frac{\omega_A}{\frac{360^\circ}{2^N-1}} = \frac{\left(2^N-1\right)\times\omega_A}{360^\circ}. \tag{14}$$

where α_D is the grating pitch of the auxiliary track (A), and

$$\eta_C = \frac{\omega_C}{\alpha_C} = \frac{\omega_C}{\frac{360^\circ}{2^N-2^M}} = \frac{\left(2^N-2^M\right)\times\omega_C}{360^\circ}. \tag{15}$$

where α_C is the grating pitch at the correcting track (C).

3.2. Angular information combined algorithm

According to the angular variation principle discussed in Sections 2 and 3.1, the difference in marking lines among the datum track (D), auxiliary track (A), and correcting track (C) reveals the current angular displacement information.

The angular displacement of the image detector reference line L is normalized to the incomplete grating period corresponding to angular displacement on tracks (D), (A), and (C), respectively, as η_D, η_A, η_C. The displacement can then be derived by Eqs. (1), (2), (6) and Eqs. (12), (14), (15).

$$\eta_D - \eta_A = \frac{\theta}{360^\circ} - (p - q). \tag{16}$$

$$\eta_D - \eta_C = 2^M \times \frac{\theta}{360^\circ} - (p - r). \tag{17}$$

where θ is an absolute angular position. The relationship between η_D–η_A, η_D–η_C, and θ according to the theories presented in Section 2.2 is shown in Fig. 5.

As shown in Fig. 5, in the entire circumference, η_D–η_A and θ change in a single cycle; η_D–η_C and θ change periodically over 2^M cycles.

When calculating angle information data, map η_D to 2^n so the angular displacement corresponding to ω_D is:

$$\varphi_0 = \eta_D \times 2^n. \tag{18}$$

According to the result of Eq. (5), the difference between η_D and η_C varies in a single cycle over the circumference. When calculating the angle information, the difference is mapped to 2^M.

$$\Delta\varphi_1 = (\eta_D - \eta_A) \times 2^M. \tag{19}$$

Similarly, according to the result of Eq. (8), the difference between η_D and η_C varies by 2^M cycles over the circumference.

$$\Delta\varphi_2 = (\eta_D - \eta_C) \times 2^{N-M}. \tag{20}$$

Per the theories presented in Section 2.2, the N-bit coarse code information can be determined by $\triangle\varphi_1$, $\triangle\varphi_2$, where the lower (N-M)-bit information is determined by $\triangle\varphi_2$ and the higher M-bit information is determined by $\triangle\varphi_1$. The n-bit fine code information of the absolute angular position is determined by φ_0. Next, φ_0 is spliced with $\triangle\varphi_2$, and $\triangle\varphi_1$ is spliced with $\triangle\varphi_2$ by phase correction method. The angular position information detected by the current image detector is connected to the data. Fig. 6 shows the angle information constituting the model, where "*DATA*" is the angle data as-obtained.

3.3. Code correction method

Scribed error in the grating code disk as well as in the installation and debugging of the device can cause deviation of the edge position of the reticle from the theoretical position. The relative angle between two lines trace is difficult to ensure, and may cause a wrong code when $\triangle\varphi_1$ and $\triangle\varphi_2$ or when $\triangle\varphi_2$ and φ_0 are connected. When φ_0 is carried or borrowed, the lowest 1 bit of $\triangle\varphi_2$ changes in advance or is delayed; when $\triangle\varphi_2$ carries or borrows, the lowest 1 bit of $\triangle\varphi_1$ similarly changes early or is delayed.

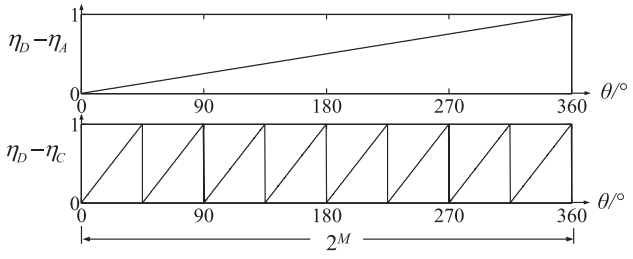

Fig. 5. Relationship between η_D–η_A, η_D–η_C, and θ.

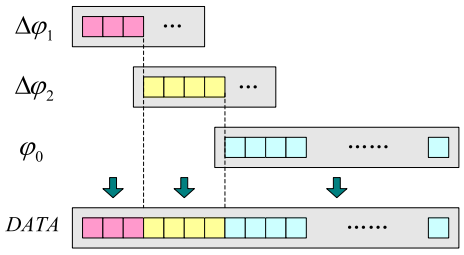

Fig. 6. Angle combined model.

To implement the correction algorithm, according to Eqs. (19) and (20), let $\triangle\varphi_1 = (\eta_D - \eta_A) \times 2^{M+1}$ and $\triangle\varphi_2 = (\eta_D - \eta_C) \times 2^{(N-M)+1}$.

- The correction algorithm between $\triangle\varphi_2$ and φ_0 is as follows:

When the lowest bit of $\triangle\varphi_2$ is "1", the upper two bits of φ_0 are "00", indicating that $\triangle\varphi_2$ leads to φ_0, then let $\triangle\varphi_2 = \triangle\varphi_2 - 1$;
When the lowest bit of $\triangle\varphi_2$ is "0", the upper two bits of φ_0 are "11", indicating that $\triangle\varphi_2$ lags behind φ_0, then let $\triangle\varphi_2 = \triangle\varphi_2 + 1$.

- The correction algorithm between $\triangle\varphi_1$ and $\triangle\varphi_2$ is as follows:

When the lowest bit of $\triangle\varphi_1$ is "1", the upper two bits of $\triangle\varphi_2$ are "00", indicating that $\triangle\varphi_1$ leads to $\triangle\varphi_2$, then let $\triangle\varphi_1 = \triangle\varphi_1 - 1$;
When the lowest bit of $\triangle\varphi_1$ is "0", the upper two bits of $\triangle\varphi_2$ are "11", indicating that $\triangle\varphi_1$ lags behind $\triangle\varphi_2$, then let $\triangle\varphi_1 = \triangle\varphi_1 + 1$.
According to the value after the correction algorithm, the data can be reconnected as shown in Fig. 6.

4. Errors analysis

The sources of angular error measurement in the proposed device mainly originate from acquisition, subdivision calculation, and grating disk eccentricity. Acquisition error is caused by the image blur when the axis rotation speed is too fast. Subdivision calculation error is derived from the approximation during subdivision angle calculation. Code disk eccentricity error is caused by the difference between the grating code disk and the axis.

The angular displacement measurement technique discussed here is in the static state, so acquisition error can be neglected. The centroid algorithm and the code value correction method adopted here weaken the impact of subdivision error on the measurement result to the point of negligibility.

When the grating disk is installed, there is an eccentricity of e, the phase angle between the direction of eccentricity and the direction of absolute zero position is γ, grating disk radius of R, and measured absolute angular position is θ_s. The angular displacement error caused by the eccentricity is [23]:

$$\mu = \arctan\left(\frac{e \times \sin(\theta_s - \gamma)}{R + e \times \cos(\theta_s - \gamma)}\right) \times \frac{180^\circ}{\pi}. \tag{21}$$

When the grating disk radius is small, the eccentricity error has a significant influence on the angular displacement measurement.

5. Experiments

We built a small prototype of the proposed image-type angular displacement measurement device as shown in Fig. 7. The setup includes an image detector, disk, light, flange, and axis.

The distance between the image detector and the grating is extremely small. The diameter of the grating code disk is 38 mm. The effective imaging area size of the image detector is 1280 × 1024, and the image detection area size for setting three respective code channels is 640 × 1.

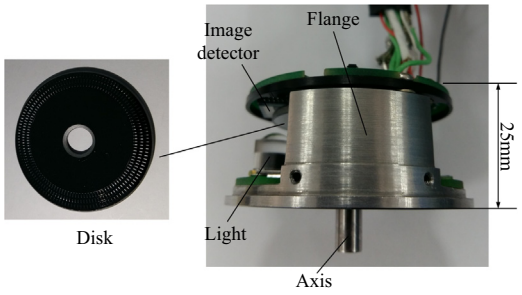

Fig. 7. Measuring equipment.

In this study, we adopted a decoupling process in the hardware circuit to enhance the anti-interference capability of the measurement system. We also used the centroid algorithm to smooth the image during the sub-pixel positioning process. The anti-interference of the measuring device is guaranteed by the software.

5.1. Resolution test

We used image detectors to identify the three code channels of the raster code and uploaded to the upper computer software for display, as shown in Fig. 8.

In Fig. 8, L is the image detector reference line and the position is 320. A_A, B_A, A_D, B_D, A_C, and B_C are the centroid of the grating marking lines on both sides of the reference line, respectively; C_A, C_D, and C_C are the intersection points of the lines A_AB_A, A_DB_D, A_CB_C, and the reference line L; $N = 7$, $M = 3$, and $n = 13$ were obtained by the coding method. It is possible to obtain$\triangle\varphi_1$, $\triangle\varphi_2$ and φ_0, respectively, under the theories described above. Then:

$$\varphi_0 = \frac{2^N}{2\pi} \times \arctan\frac{B_DC_D}{OC_D} \times 2^{13}. \tag{22}$$

$$\Delta\varphi_1 = \frac{2^N}{2\pi} \times \left(\arctan\frac{B_DC_D}{OC_D} - \arctan\frac{B_AC_A}{OC_A}\right) \times 2^3. \tag{23}$$

$$\Delta\varphi_2 = \frac{2^N}{2\pi} \times \left(\arctan\frac{B_DC_D}{OC_D} - \arctan\frac{B_CC_C}{OC_C}\right) \times 2^4. \tag{24}$$

In Eqs. ((22)–(24)), OC_A, OC_D, and OC_C are the lines connecting the code center O and C_A, C_D, and C_C, which are the image detector on the datum track (D), auxiliary track (A), and correcting track (C) corresponding to the distance of the line from the axis. $\triangle\varphi_1$ is the upper 3-bit data of *DATA*, $\triangle\varphi_2$is the middle 4-bit data of *DATA*, and φ_0 is the lower 13-bit data of *DATA*.

$$DATA = \Delta\varphi_1 \times 2^{17} + \Delta\varphi_2 \times 2^{13} + \varphi_3. \tag{25}$$

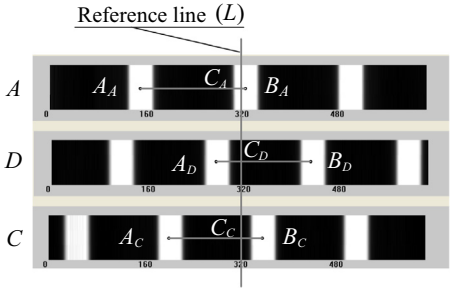

Fig. 8. Disk information.

We next slowly rotated the axis and observed the error-free code. The angular displacement measuring device provided 20-bit resolution in our test.

5.2. Precision test

We next applied a high-precision angle reference method to determine the accuracy of the proposed device, as shown in Fig. 9. We measured the test device with a large, 24-bit reference photoelectric encoder which has precision of 1″ and resolution of 0.07″.

In Fig. 9, the angle reference was connected to the device to be inspected through coupling. The angle reference was rotated coaxially with the posing device throughout the detection process. The data of the two devices were recorded every 15°; the difference between the two sets of data is the error. We performed three independent test experiments (Fig. 10).

As shown in Fig. 10, in one rotation cycle of the angular displacement measuring device, the maximum mean-square deviation is 55″ and the minimum mean-square deviation is −45″. The average of the three test results representative of the accuracy of the proposed device is shown in Table 1.

The mean-square deviation of the proposed device is 20.4″ of the angular displacement.

5.3. Comparison against traditional angular displacement measuring device

We also tested a traditional angular displacement measuring device of the same size as the proposed device for the sake of comparison. The grating disk is coded in Gray code, five circles are scribed on the circumference of the disk, and angular displacement (18-bit) of 4.9″ can be recognized. The results of our comparison are shown in Fig. 11.

Compared to the traditional angular displacement measuring device of the same size, the proposed device has superior resolution by 2-bit with a smaller grating density. As shown in Fig. 11, the error in the traditional device is generally higher than that in the proposed device. After calculation, the error mean square error of the traditional device is 42.43″. By comparison, the technical specifications of the proposed small-image-type angular displacement measurement device far exceed the traditional device of the same size.

5.4. Prototype stability

We performed high (60 °C) and low (−40 °C) temperature experiments on the proposed device to test its stability. The results show that the device can be easily initialized and operates normally under both high-temperature and low-temperature conditions.

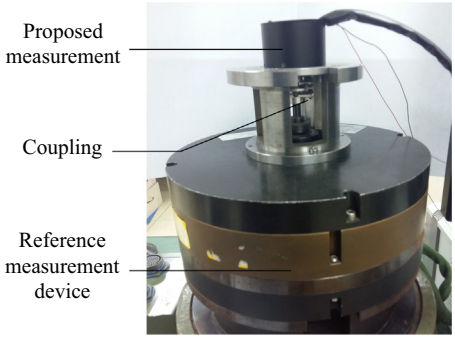

Fig. 9. Schematic diagram of experimental setup.

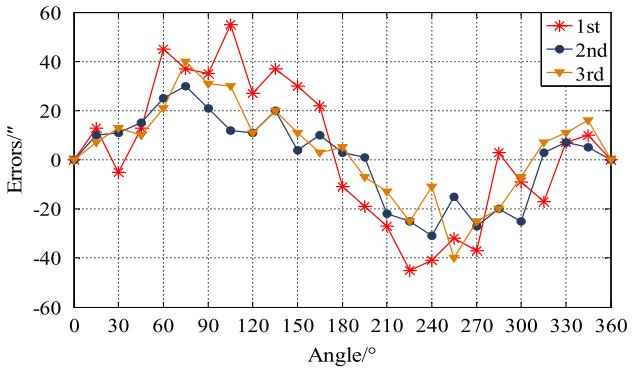

Fig. 10. Error curve.

Table 1
Detection results.

Angles	Average errors	Angles	Average errors
0°	0″	195°	−8.33″
15°	10″	210°	−20.67″
30°	6.33″	225°	−31.67″
45°	12. 67″	240°	−27.67″
60°	30.33″	255°	−29″
75°	35.67″	270°	−29.67″
90°	29″	285°	−12.33″
105°	32.33″	300°	−13.67″
120°	16.33″	315°	−2.33″
135°	25.67″	330°	8.33″
150°	15″	345°	10.33″
165°	11.67″	360°	0″
180°	−1″		

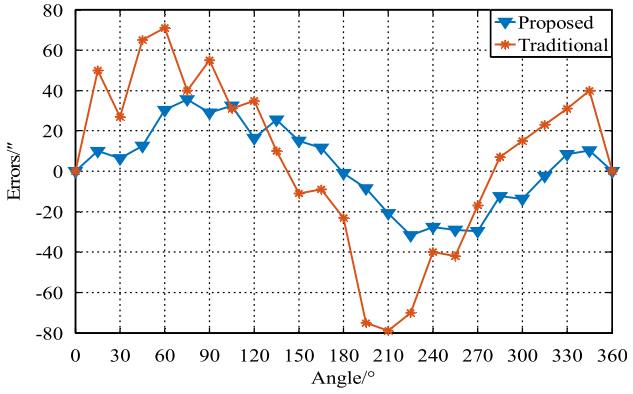

Fig. 11. Error by contrast.

6. Conclusion

This paper proposed a small-image-type angular displacement measuring device and introduced its system structure and measurement principle in detail. A 38-mm diameter grating disk was designed and encoded using the varying principle, then three lines of single-line pixel data were detected separately to enhance the system response frequency, and a sub-pixel level angular displacement calculation model was established based on lens-free near-field imaging. A combination angle information algorithm and a code correction method were written for the proposed setup. Error analysis was also performed. A prototype of the proposed angular displacement measuring device achieved 20-bit resolution and 20.4″ accuracy. Further, its technical indicators were found to be better than a traditional angular displacement measuring device of the same size.

The technology and sub-pixel varying principle discussed in this paper may represent a workable foundation for future research on small-size, high-precision, high-resolution angular displacement measurement devices.

Acknowledgements

This study was funded by the National Natural Science Foundation of China (NSFC) (No. 51605465). This project was also supported by the Science and Technology Development Programme of Jilin province (No. 20180520184JH).

References

[1] Q. Lv, W.H. Li, Bayinhexige,, et al., Interferometric precision displacement measurementsystem based on diffraction grating, Chinese Optics 10 (1) (2017) 39–50 (in Chinese).
[2] H.B. Zhang, Q.H. Wan, S.J. Wang, et al., Installation error control of dynamic measurement for small photoelectric encoder, Optics Precis. Eng 24 (7) (2016) 1655–1660 (in Chinese).
[3] G. Ye, S. Fan, H. Liu, et al., Design of a precise and robust linearized converter for optical encoders using a ratiometric technique, Meas. Sci. Technol. 25 (12) (2014) 125003.
[4] G. Ye, H. Liu, Y. Wang, et al., Ratiometric-linearization-based high-precision electronic interpolator for sinusoidal optical encoders, IEEE Trans. Ind. Electron. 65 (10) (2018) 8224–8231.
[5] Oleg U. Lashmanova, Aleksandr S. Vasileva, Anna V. Vasileva, et al., High-precision absolute linear encoder based on a standard calibrated scale, Measurement 123 (2018) 226–234.
[6] G.Y. Ye, H.Z.H. Liu, Y.W. Ban, et al., Development of a reflective optical encoder with submicron accuracy, Opt. Commun. 411 (2018) 126–132.
[7] J.L. Deng, X.N. Yan, C.H.L. Wei, et al., Eightfold optical encoder with high-densityGrating, Appl. Opt. 57 (10) (2018) 2366–2376.
[8] Douglas B. Leviton. New ultra-high sensitivity, absolute, linear, and rotary encoders. Proc. of SPIE Vol. 3440:100-111.
[9] Douglas B. Leviton, Bradley J. Frey., Ultra-high resolution, absolute position sensors for cryostaticapplications, Proc. of SPIE 4850 (2003) 776–787.
[10] Jovan S. Bajić, Dragan Z. Stupara, Bojan M. Dakićb, et al., An absolute rotary position sensor based on cylindrical coordinate color space transformation, Sens. Actuat. A Phys. 213 (2014) 27–34.
[11] Hyuno Kim, Yuji Yamakawa, Taku Senoo, et al., Visual encoder: robust and precisemeasurement method of rotation anglevia high-speed RGB vision, Appl. Opt. 12 (2016) 13375–13386.
[12] Yukinobu Sugiyama, Yoshinori Matsui, Haruyoshi Toyoda, et al., A 3.2 kHz, 14-bit optical absolute rotary encoder with a CMOS profile sensor, IEEE Sens. J. 8 (8) (2008) 1430–1436.
[13] M. Tresanchez, T. Pallejà, M. Teixidó, J. Palacín, The optical mouse sensor as an incremental rotary encoder, Sens. Actuat. A Phys. 155 (2010) 73–81.
[14] M. Tresanchez, T. Pallejà, M. Teixidó, J. Palacín, Using the image acquisition capabilities of the optical mouse sensor to build an absolute rotary encoder, Sens. Actuat. A 157 (2010) 161–167.
[15] Jae Wan Jong-AhnKima, Chu-Shik Kang Kima, et al., Absolute angle measurement using a phase-encoded binarygraduateddisk, Measurement 80 (2016) 288–293.
[16] Xu. Jin, Ye Wentong, Ni Xuxiang, et al., Virtual moiré fringe for grating measurement system based on CMOS microscopic imaging, Proc. of SPIE 785325 (2010) 1–5.
[17] H. Yu, Q.H. Wan, X.R. Lu, et al., Small-size, high-resolution angular displacementmeasurement technology based on an imagingdetector, Appl. Opt. 56 (3) (2017) 755–760.
[18] H. Yu, Q.H. Wan, L.H. Ling, et al., An error compensation arithmetic of angular displacement measurement via dual imaging detectors, Opt. Eng. 57 (5) (2018) 054108.
[19] Ariel Lutenberg, Fernando Perez-Quintián, María A. Rebollo, Optical encoder based on a nondiffractive beam, Appl. Opt. 47 (13) (2008) 2201–2206.
[20] M.S. Wei, F. Xing, Zh You, A real-time detection and positioning method for small and weak targets using a 1D morphology-based approach in 2D images, Light Sci. Appl. 7 (2018) 18006.
[21] H.W. Chen, Jiun-Haw Lee, Bo-Yen Lin, Liquid crystal display and organic light-emitting diode display: present status and future perspectives, Light Sci. Appl. 7 (2018) 17168.
[22] Yair Rivenson, Yibo Zhang, Harun Günaydın, et al., Phase recovery and holographic image reconstruction using deep learning in neural networks, Light Sci. Appl. 7 (2018) 17141.
[23] A.I. Chg, C.H.U. Su, X. Han, et al., Eccentric testing of benchmark circular grating and compensation of angular error, Optics Precis. Eng. 21 (10) (2012) 2479–2484.